Journal of Materials Science: Materials in Electronics (2019) 30:10217–10223
https://doi.org/10.1007/s10854-019-01358-1

New negative temperature coefficient ceramics in La-doped $CaCu_3Ti_4O_{12}$ system

Xuemei Jia[1,2] · Bo Zhang[1] · Aimin Chang[1]

Received: 31 January 2019 / Accepted: 16 April 2019 / Published online: 27 April 2019

Abstract
The $Ca_{1-x}La_xCu_3Ti_4O_{12}$ ($0 \le x \le 0.3$) ceramics have been successfully prepared by the traditional solid-state reaction method at 1090 °C for 10 h. Effects of La^{3+} doping on the structure and negative temperature coefficient electrical properties of $Ca_{1-x}La_xCu_3Ti_4O_{12}$ ceramics are investigated in detail. Scanning electron microscope images demonstrate that the grain size of ceramic samples decreases with the increasing La^{3+} content. X-ray photoelectron spectroscopy analysis further confirms the coexistence of Cu^+/Cu^{2+} and Ti^{3+}/Ti^{4+} ions, which is one of the considerable contributors to the electrical conductivity of $Ca_{1-x}La_xCu_3Ti_4O_{12}$ ceramics. All the prepared ceramics show a linear relationship between the natural logarithm of the resistivity and the reciprocal of absolute temperature, indicating NTC characteristics. The obtained values of ρ_{25}, $B_{200/400}$ and Ea for the thermistors are in the range of 2.00×10^5–5.22×10^7 Ω cm^{-1}, 2644–4205 K, 0.228–0.363 eV, respectively.

1 Introduction

Negative temperature coefficient (NTC) thermistors are thermally sensitive resistors whose resistance exhibits a decrease as temperature increases. A necessary condition for their NTC behavior is the electron jump between neighbour ions of the same type and having different valences [1, 2]. NTC thermistors are widely used for aerospace, temperature compensation and control [1]. Classical NTC materials usually consist of transition metal oxides with spinel structure (AB_2O_4) [3].

Lately, there has been a rising interest in studying NTC behavior of complex oxide materials for thermistor applications. The perovskite-like material $CaCu_3Ti_4O_{12}$ (CCTO) has been widely studied owing to its interesting dielectric properties [4–9]. The high dielectric constant of CCTO enable it to be considered as a potential candidate for microelectronic applications such as resonators, filters and cellular phones [7, 9, 10]. Moreover, after comprehensive investigations into its intrinsic mechanism, the hints to the giant dielectric constant of CCTO are focused on the Internal Barrier Layer Capacitance mechanism, suggesting that CCTO ceramic is composed of semiconducting grains and insulating grain boundaries [11], a necessary condition for NTC behavior. What's more, CCTO contains oxygen deficiencies, which can be compensated by low-valence Ti^{3+} and Cu^+ ions [12]. Bearing in mind that it has the characteristic of semiconductivity, CCTO material can be used for NTC thermistors. However, previous researches on CCTO mostly focus on improving its dielectric and nonlinear electrical properties by element doping [10, 13–15]. We have investigated the NTC electrical performances and conduction mechanism of Cu-sited doped CCTO ($CaCu_{3-x}Mn_xTi_4O_{12}$) ceramics [16]. Based on previous work, considering the ionic radii of Ca^{2+} (1.34 Å) and La^{3+} (1.36 Å) [17] with 12-fold coordination number are similar, we propose that by doping La^{3+} ions on Ca sites, solid solutions can be formed and the NTC electrical properties of CCTO can be adjusted. The main aim in the present work is to research the effect of La^{3+} doping on the structure and NTC electrical performance of Ca-sited doped $CaCu_3Ti_4O_{12}$ ceramics.

✉ Bo Zhang
zhangbocas@ms.xjb.ac.cn

✉ Aimin Chang
changam@ms.xjb.ac.cn

[1] Key Laboratory of Functional Materials and Devices for Special Environments of CAS; Xinjiang Key Laboratory of Electronic Information Materials and Devices, Xinjiang Technical Institute of Physics & Chemistry of CAS, Urumqi 830011, China

[2] University of Chinese Academy of Sciences, Beijing 100049, China

1.1 Experiment

The $Ca_{1-x}La_xCu_3Ti_4O_{12}$ ($x = 0.0$, 0.1, 0.2, 0.3) polycrystalline samples were synthetized by the traditional solid-state method. The starting materials were $CaCO_3$ (≥ 99%), La_2O_3(≥ 99.99%), CuO (≥ 99%) and TiO_2 (≥ 99.0%). The raw materials were weighed on the basis of their stoichiometric ratio and ground in mortar for 6 h. Then the powders were calcined at 900 °C in air for 6 h. The calcined powders were then pressed into the cylindrical pellets with about 10 mm in a diameter, then cold isostatic pressing at 300 MPa was used to improve density. All the pellets were sintered at 1090 °C for 10 h.

The crystal structure of as-sintered specimen is studied by X-ray diffraction (XRD; BRUKERD8-ADVANCE, Cu K_α radiation) analysis. The surface microstructure and the compositional distribution of the ceramic samples were analyzed by the Scanning Electron Microscope (SEM; Zeiss SUPRA 55 VP, Germany) in combination with energy dispersive spectroscopy (EDS). X-ray Photoelectron Spectroscopy (XPS; Thermo Scientific, K-Alpha +) was adopted to investigate the chemical states of the ceramic samples. So as to obtain the electrical conductivity, the both parallel sides of the ceramics were coated with platinum paste, and then annealed at 800 °C for 30 min. The relationship between resistances and temperature were measured from 25 up to 400 °C by a digital multimeter.

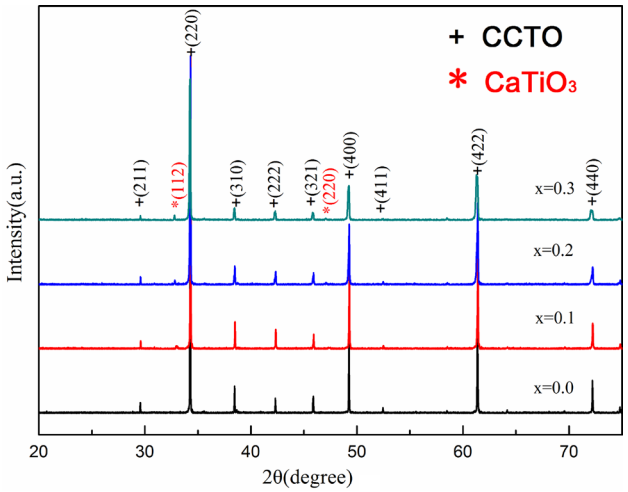

Fig. 1 XRD patterns of the $Ca_{1-x}La_xCu_3Ti_4O_{12}$ ceramics after sintering at 1090 °C for 10 h

Table 1 Lattice constant, ρ_{25}, B constant and activation energy (Ea) of the $Ca_{1-x}La_xCu_3Ti_4O_{12}$ ceramics

x	a (Å)	ρ_{25} (Ω cm^{-1})	$B_{200/400}$ (K)	Ea (eV)
0	7.3942	5.22×10^7	4205	0.363
0.1	7.3947	3.42×10^6	3775	0.326
0.2	7.3968	4.35×10^5	3252	0.281
0.3	7.4050	2.00×10^5	2644	0.228

2 Results and discussion

Figure 1 shows the XRD patterns of $Ca_{1-x}La_xCu_3Ti_4O_{12}$ ceramics sintered at 1090 °C for 10 h. All the diffraction peaks in XRD patterns for all samples were completely indexed to be the CCTO phase having a body-centered cubic structure with space group Im-3. The structure was refined by using TOPAS. Lattice constant of the $Ca_{1-x}La_xCu_3Ti_4O_{12}$ ceramics is listed in Table 1. From the Table 1, it can be seen that the lattice constant increased with increasing La content. This result can be understood based on the fact that the substitution of larger La^{3+} for Ca^{2+} causes a lattice expansion and thereby resulting in an increase in the lattice constant. But a small amount of secondary phase ($CaTiO_3$) was also detected in the La^{3+}-doped CCTO ceramics. The appearance of $CaTiO_3$ may be relevant to the liquid phase sintering mechanism of CCTO and the doping of La^{3+}. The sintering mechanism of CCTO suggests that the rate of grain growth of CCTO ceramics is inhibited by $CaTiO_3$ solid particles, and the second phase $CaTiO_3$ can be incorporated into CCTO lattices to form a solid solution in the last stage of sintering processes [18], which is in accordance with following SEM results. The doping of La^{3+} may reduce the solid solubility limit of $CaTiO_3$ in CCTO ceramics, and result in the appearance of second-phase $CaTiO_3$.

The SEM morphology of the polished and thermally etched surfaces of ceramic specimens is shown in Fig. 2. The specific process of thermal etching for the ceramic samples is as follows: the polished ceramic samples were thermally etched at 950 °C for 40 min in air atmosphere. It can be seen that the substitution of La^{3+} for Ca^{2+} has an obvious effect on the microstructure of CCTO ceramics. Discontinuous grain growth occurred in all the ceramic samples, and the terrace-ledge and bump area morphologies observed on the grain surfaces for the ceramics may result from a spiral growth of crystals by screw dislocation [5]. This morphology is present under thermal etching, and is easy to develop at lower etching temperatures or shorter etching times [5]. It is also noted that the grain size of ceramic samples decreased with the increasing La^{3+} content. This is mainly attributed to the appearance of second-phase $CaTiO_3$ produced by the doping of La^{3+}, which impedes the movement of grain boundaries, thus reducing the growth of grains. This result is agreement with the discussion based on the XRD results. From Fig. 2, it can be seen that there is a pore in the

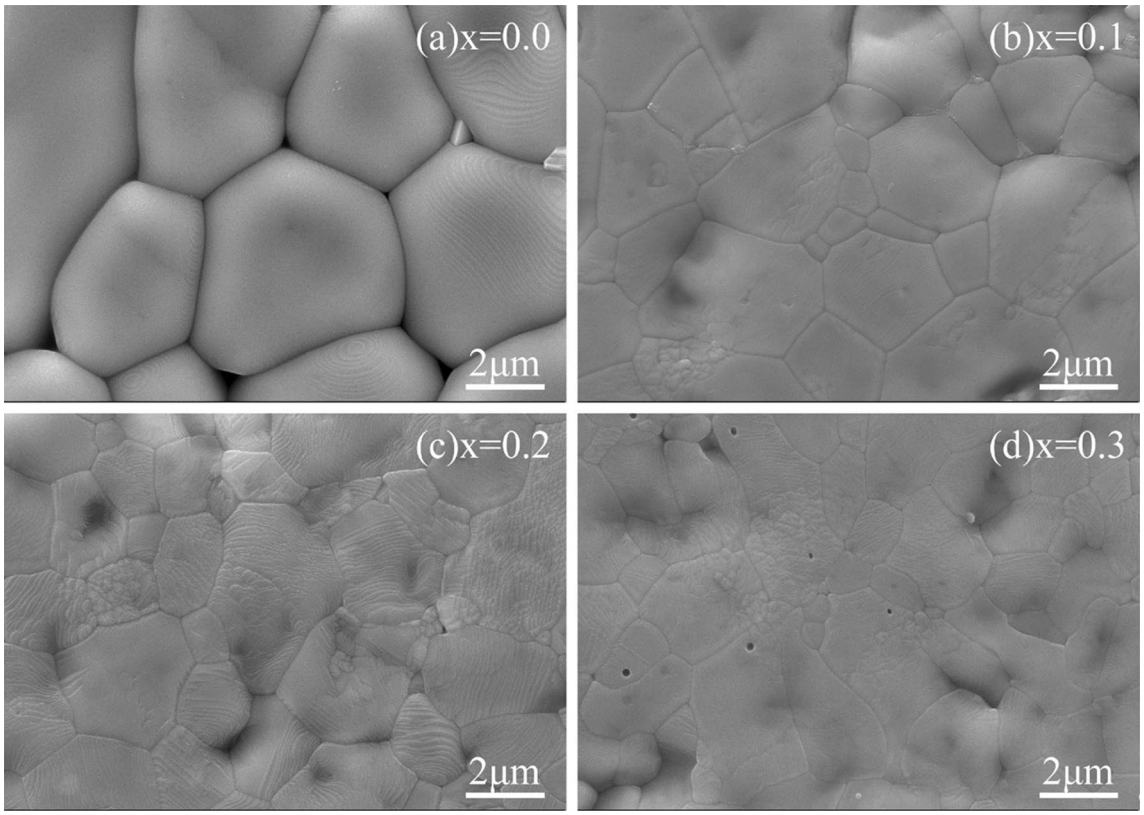

Fig. 2 SEM images obtained from the surfaces of the $Ca_{1-x}La_xCu_3Ti_4O_{12}$ ceramics

$Ca_{0.7}La_{0.3}Cu_3Ti_4O_{12}$ ($x=0.3$) ceramic samples. This result can be explained as follows [19]: with the assist of liquid phase, the rate of grain boundary movement is significantly larger than that of pore migration, which may result in the generation of residual pores.

The EDS analysis was used to confirm the compositional distributions of the $Ca_{1-x}La_xCu_3Ti_4O_{12}$ ceramics. The atomic percentages of elements are listed in Table 2 where the molar ratio is also presented. From the Table 2, it can be seen that the ratio of Ca/La is close to the stoichiometric ratio, which is consistent with our experimental design.

Figure 3 shows the fitted XPS results of Cu $2p_{3/2}$. The peaks with highest and intermediate energy correspond to Cu^{2+}, and the highest binding energy is attributed to the coordination of Cu^{2+} with six oxygen atoms [20]. The lowest binding energy states of three components of Cu $2p_{3/2}$ peak are attributed to Cu^{+} [21]. These results identify the existence of Cu^{+} and Cu^{2+} in ceramic specimens. From Fig. 3, we can obtain the Cu $2p_{3/2}$ curve-fitted line which is a superposition of lines of the calibration compounds with Cu^{+} and Cu^{2+}, as shown in Fig. 4. It can be seen that peak positions of Cu $2p_{3/2}$ exhibited a chemical shift to lower binding energy with increasing La^{3+} contents, suggesting an increase in the concentration of Cu^{+} ions.

Ti 2p XPS spectra are shown in Fig. 5. The peaks of $2p_{3/2}$ and $2p_{1/2}$ peaks can be divided into two peaks, suggesting the contribution from Ti^{3+} and Ti^{4+}. These results are in accordance with previous studies [22]. From Fig. 5, we can obtain the Ti $2p$ curve-fitted line which is a superposition of lines of the calibration compounds with Ti^{3+} and Ti^{4+}, as shown in Fig. 6. It can be seen that peak positions of Ti $2p$ exhibited a chemical shift to lower binding energy with

Table 2 Atomic percentages and molar ratio of elements in $Ca_{1-x}La_xCu_3Ti_4O_{12}$ ceramics

x	Atomic percentages of elements (at.%)					Molar ratio
	Ca	La	Cu	Ti	O	
0	5.00	–	13.75	22.21	60.04	Ca:Cu:Ti:O = 1.00:2.75:4.44:12.00
0.1	4.80	0.37	14.27	21.57	58.99	Ca:La:Cu:Ti:O = 0.93:0.07:2.76:4.17:11.41
0.2	4.17	1.29	14.74	20.83	58.98	Ca:La:Cu:Ti:O = 0.76:0.24:2.70:3.82:10.80
0.3	3.39	1.36	13.79	19.33	62.13	Ca:La:Cu:Ti:O = 0.71:0.29:2.90:4.07:13.08

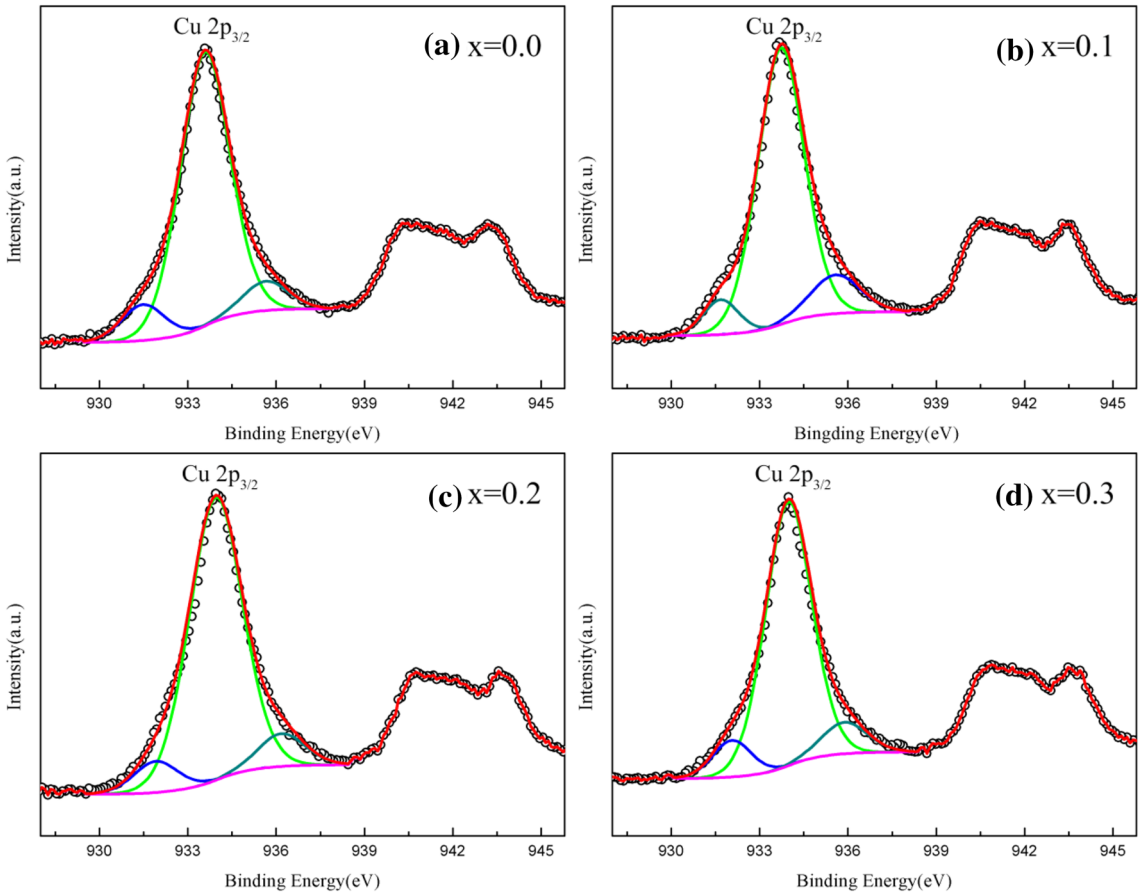

Fig. 3 Cu $2p_{3/2}$ XPS spectra collected for $Ca_{1-x}La_xCu_3Ti_4O_{12}$ ceramics

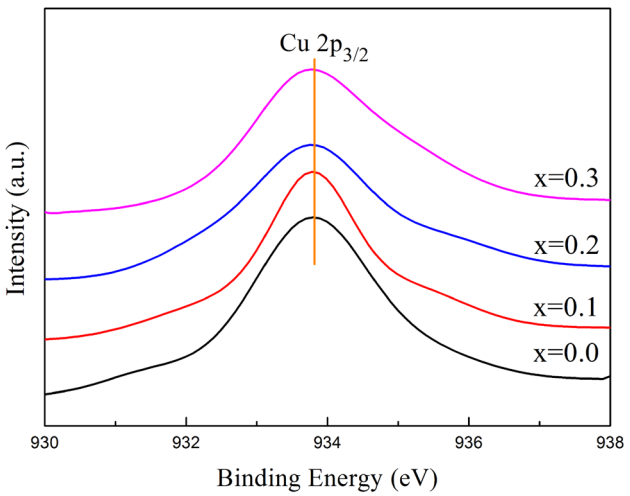

Fig. 4 XPS spectra of Cu $2p_{3/2}$ curve-fitted line derived from the superposition of lines of the calibration compounds with Cu^+ and Cu^{2+} for $Ca_{1-x}La_xCu_3Ti_4O_{12}$ ceramics

increasing La^{3+} contents, suggesting an increase in the concentration of Ti^{3+} ions.

The plots of natural logarithm of the resistivity ($\ln\rho$) dependence on the reciprocal absolute temperature ($1000/T$) for the NTC thermistors are shown in Fig. 7. As can be seen the resistivity decreased with increasing temperature, indicating the NTC behavior. It is also pointed out that the relationship between the $\ln\rho$ and $1000/T$ is approximate in linear over the measurement region of temperature. The linearity is based on the small polaron hopping transport model [23], which is able to be expressed by the following equation: $\rho = \rho_0 \exp(Ea/kT)$, where ρ_0 is the resistivity as the temperature tends to infinity, Ea is the activation energy, k is the Boltzmann constant, and T is the absolute temperature. According to previous study [24], the electronic transport for CCTO is described by small-polaron hopping which is able to be explained as follows: (1) Cu^{2+} becomes non-stable and reduces to Cu^+ during the heating process, which can be compensated by the substitution of Ti^{4+} on the Cu site to maintain the charge balance. This procedure can be described by the reaction $Ti_{Ti}^{\times} + 2Cu^{2+} \rightarrow 2Cu^{+} + Ti_{Cu}^{\cdot\cdot}$; (2) The Cu^+

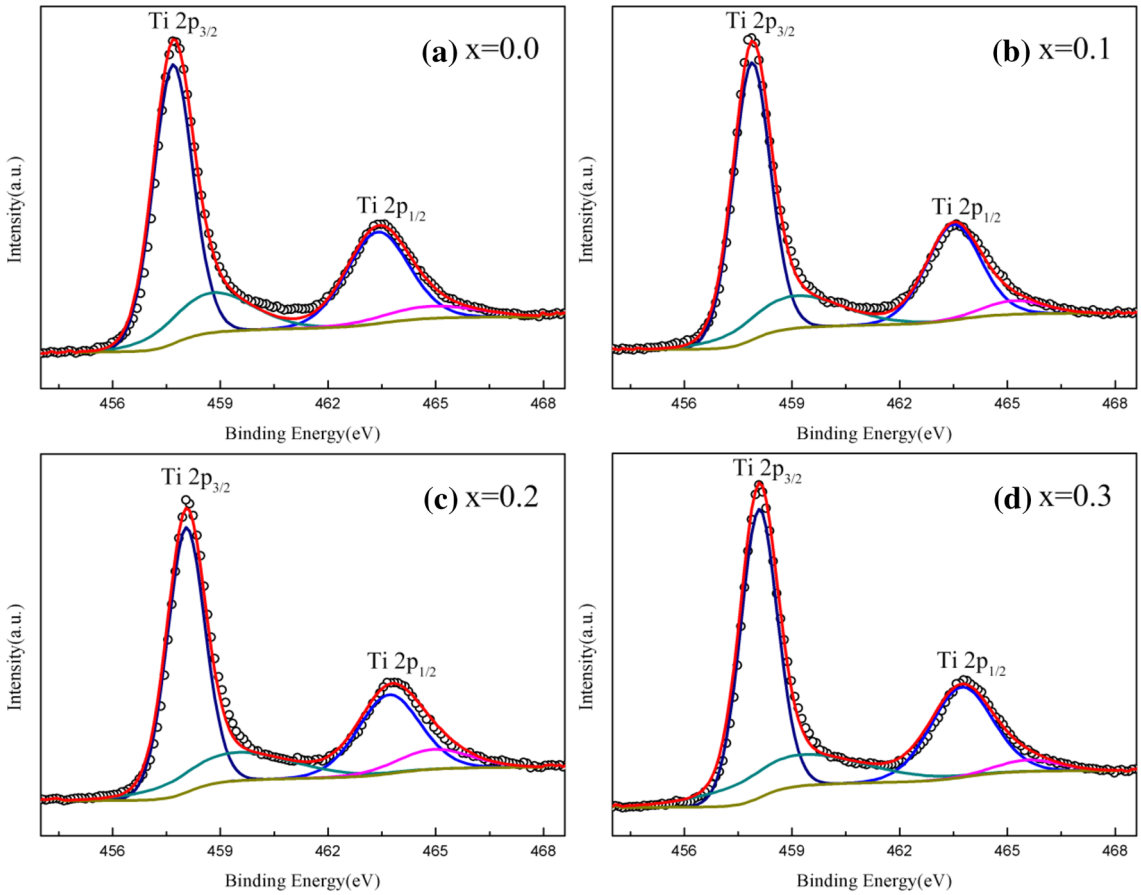

Fig. 5 XPS spectra of Ti 2*p* regions of $Ca_{1-x}La_xCu_3Ti_4O_{12}$ ceramics

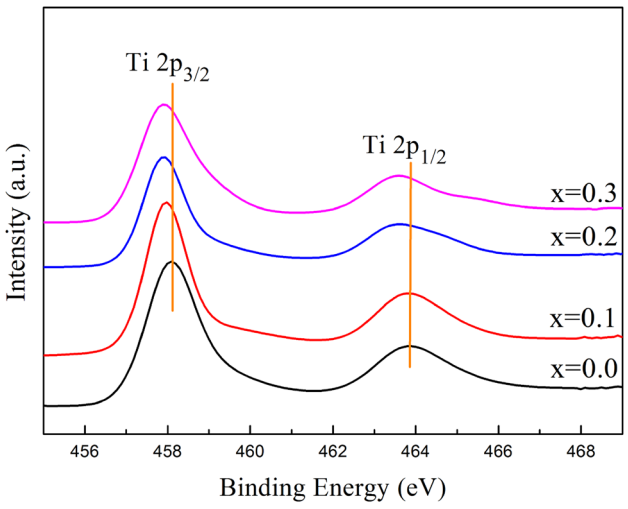

Fig. 6 XPS spectra of Ti 2*p* curve-fitted line derived from the superposition of lines of the calibration compounds with Ti^{3+} and Ti^{4+} for $Ca_{1-x}La_xCu_3Ti_4O_{12}$ ceramics

will re-oxidized to Cu^{2+} to accompanied by the released electrons entering the Ti 3d conduction band when cooling down, which results in the reduction of Ti^{4+}–Ti^{3+}. The expression of this process can use the reaction $Cu^{+} + Ti^{4+} \rightarrow Cu^{2+} + Ti^{3+}$. This explanation indicates that the major carrier is electron and CCTO is a n-type semiconductor [25–27]. Thus, small-polaron hopping transport mechanism for the CCTO is attributed to the electron hopping between the Cu^{2+} and Cu^{+} cations, and between Ti^{4+} and Ti^{3+} cations. Besides, we can detect that the resistivity reduced with rising La^{3+} content. When La^{3+} substitutes for Ca^{2+}, there is a formation of electron, which results in a higher electron concentration, thereby reducing the energy barrier for polaron hopping, and reducing the resistivity. That is to say, the substitution of La^{3+} for Ca^{2+} promotes the conversion of Cu^{2+}–Cu^{+} and Ti^{4+}–Ti^{3+}. The defect formation mechanism can be formulated by the reactions: $La_2O_3 \rightarrow 2La_{Ca}^{\cdot} + 2e' + 3O_O^{\times}$, $Cu^{2+} + e' \rightarrow Cu^{+}$, $Ti^{4+} + e' \rightarrow Ti^{3+}$. The results presented herein are consistent with previous XPS analysis. The increasing of Cu^{+} and Ti^{3+} concentrations will decrease the resistivity due to the n-type conductivity of the CCTO. According to our

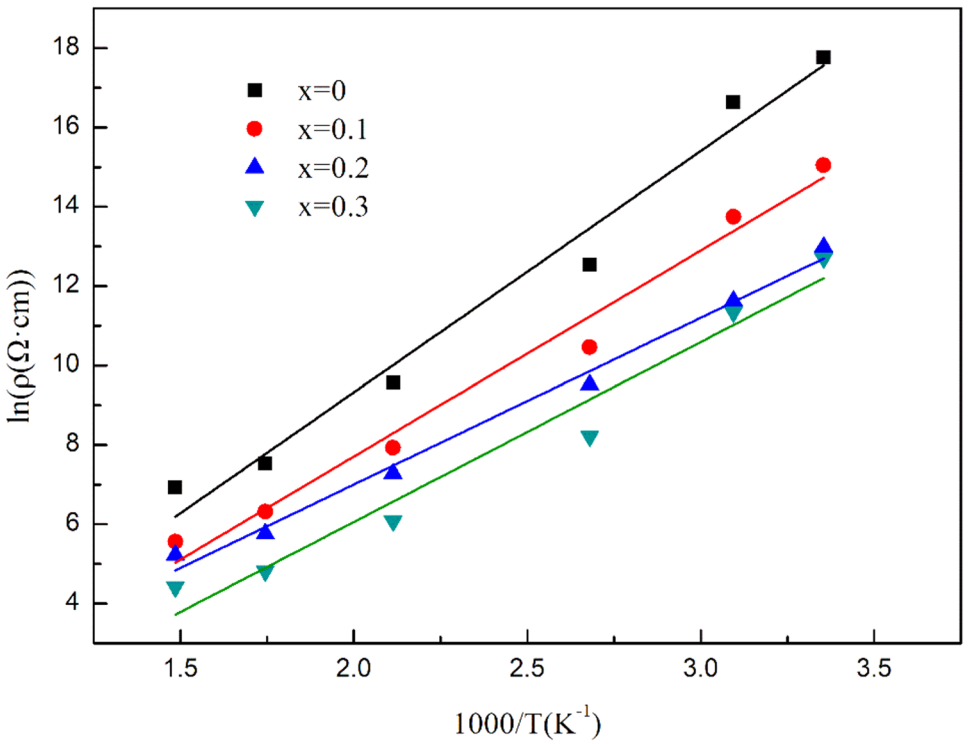

Fig. 7 Plots of the lnρ versus 1000/T for the $Ca_{1-x}La_xCu_3Ti_4O_{12}$ NTC thermistors

previous XRD results, a small amount of secondary phase $CaTiO_3$ is present in the La^{3+}-doped CCTO ceramics. The appearance of second-phase $CaTiO_3$ is in favor of the hopping conductivity due to the charge transport produced from doubly charged oxygen vacancies and electrons [28], and thus decreasing the resistivity.

The resistivity at 25 °C, $B_{200/400}$ and Ea for NTC materials are shown in Table 1. The sensitivity of thermistor material can be described by constant B which can be calculated as follows:

$$B = \left[\frac{T_1 T_2}{T_2 - T_1}\right] \ln\left(\frac{R_1}{R_2}\right)$$

where R_1 is the resistance at temperature T_1, and R_2 is the resistance at temperature T_2. As can be obtained from Table 1, the values of ρ_{25}, $B_{200/400}$ and Ea are in the range of 2.00×10^5–5.22×10^7 Ω cm^{-1}, 2644–4205 K, 0.228–0.363 eV, respectively. In addition, it can be seen that the Ea values decreased with the increasing La^{3+} content. When the La^{3+} ion is doped into the CCTO ceramics, the Cu^+ and Ti^{3+} concentrations will increase based on the following defect formation mechanism: $La_2O_3 \rightarrow 2La_{Ca}^{\cdot} + 2e' + 3O_O^{\times}$, $Cu^{2+} + e' \rightarrow Cu^+$, $Ti^{4+} + e' \rightarrow Ti^{3+}$. This results in a higher electron concentration, thereby reducing the energy barrier for polaron hopping, and thus reducing the Ea values.

Figure 8 shows the ρ_{25} and $B_{200/400}$ constant as a function of x. As shown in Fig. 8, it can be seen that the values of ρ_{25} and $B_{200/400}$ decreased with the increasing La^{3+} content. This phenomenon is due to the substitution of La^{3+} for Ca^{2+} that lowers the energy barrier for polaron hopping, thus decreasing the resistivity and B values. All the results above demonstrate that the adjustment of electrical properties of the $Ca_{1-x}La_xCu_3Ti_4O_{12}$ NTC materials can be accomplished through altering the La^{3+} content.

3 Conclusion

The crystal structure, microstructure and NTC electrical properties of $Ca_{1-x}La_xCu_3Ti_4O_{12}$ ceramics have been investigated in the present study. The major phase of as-sintered ceramics is the $CaCu_3Ti_4O_{12}$ phase. The grain size of the $Ca_{1-x}La_xCu_3Ti_4O_{12}$ ceramics decreases with increasing La^{3+} content. Through the XPS analysis, the co-existing of Cu^+/Cu^{2+} and Ti^{3+}/Ti^{4+} is confirmed, which are proposed to be the intrinsic conduction mechanism for its NTC properties. It is also found that the resistivity decreases with increasing La^{3+} content. In addition, the adjustment of electrical performance can be accomplished through altering the La^{3+} content. It is further concluded that these compounds can be applied as promising materials for NTC thermistors.

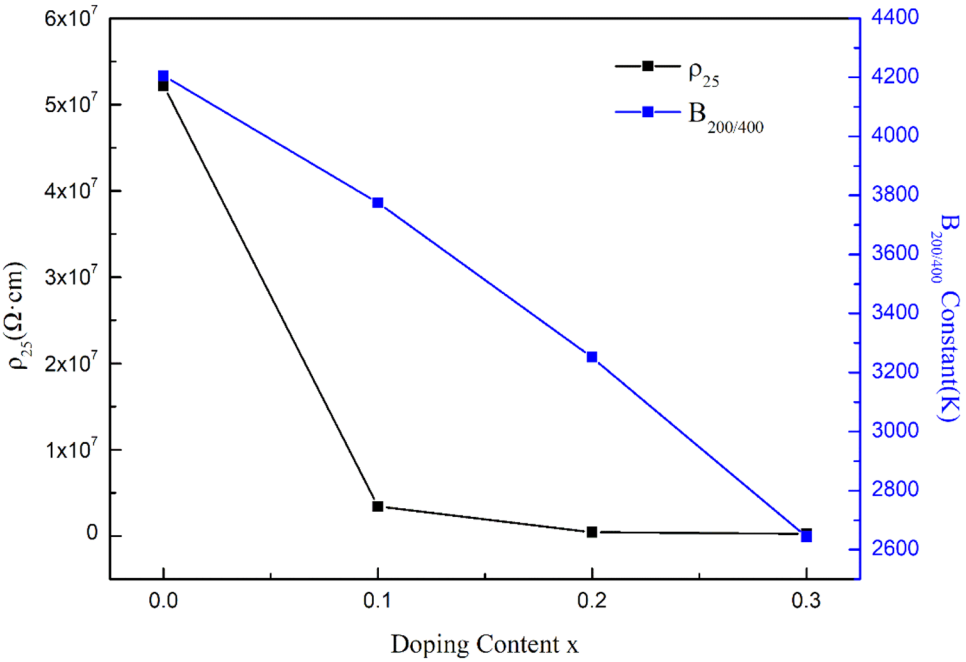

Fig. 8 Evolution of ρ_{25} and $B_{200/400}$ as a function of doping content x

Acknowledgments We would like to acknowledge financial support from the National Natural Science Foundation of China (Grant No. 61871377) and the West Light Foundation of the Chinese Academy of Sciences (Grant No. 2015-XBQN-B-13).

References

1. A. Feteira, J. Am. Ceram. Soc. **92**, 967 (2009)
2. R.N. Jadhav, S.N. Mathad, V. Puri, Ceram. Int. **38**, 5181 (2012)
3. K. Park, S. Yun, J. Mater. Sci.: Mater. Electron. **15**, 359 (2004)
4. M.A. Subramanian, D. Li, N. Duan, B.A. Reisner, A.W. Sleight, J. Solid State Chem. **151**, 323 (2000)
5. T. Fang, H. Shiau, J. Am. Ceram. Soc. **87**, 2072 (2005)
6. B.S. Prakash, K.B.R. Varma, Phys. B **382**, 312 (2006)
7. S.F. Shao, J.L. Zhang, P. Zheng, C.L. Wang, J.C. Li, M.L. Zhao, Appl. Phys. Lett. **91**, 042905 (2007)
8. Y. Zhu, J.C. Zheng, L. Wu, J. Hanson, P. Northrup, W. Ku, A.I. Frenkel, Phys. Rev. Lett. **99**, 037602 (2007)
9. B.P. Zhu, Z.Y. Wang, Y. Zhang, Z.S. Yu, J. Shi, R. Xiong, Mater. Chem. Phys. **113**, 746 (2009)
10. J. Deng, X. Sun, S. Liu, L. Liu, T. Yan, L. Fang, B. Elouadi, J. Adv. Dielectr. **06**, 1650009 (2016)
11. T.B. Adams, D.C. Sinclair, A.R. West, J. Am. Ceram. Soc. **89**, 3129 (2006)
12. L. Ni, X.M. Chen, Appl. Phys. Lett. **91**, 323 (2007)
13. N. Lei, M.C. Xiang, J. Am. Ceram. Soc. **93**, 184 (2010)
14. J. Boonlakhorn, P. Kidkhunthod, N. Chanlek, P. Thongbai, J. Eur. Ceram. Soc. **38**, 137 (2018)
15. J. Wang, Z. Lu, T. Deng, C. Zhong, Z. Chen, J. Eur. Ceram. Soc. **38**, 3505 (2018)
16. B. Zhang, Q. Zhao, A. Chang, H. Ye, S. Chen, Y. Wu, Ceram. Int. **40**, 11221 (2014)
17. M.J. Forbess, S. Seraji, Y. Wu, C.P. Nguyen, G.Z. Cao, Appl. Phys. Lett. **76**, 2934 (2000)
18. S. Vangchangyia, E. Swatsitang, P. Thongbai, S. Pinitsoontorn, T. Yamwong, S. Maensiri, V. Amornkitbamrung, P. Chindaprasirt, J. Am. Ceram. Soc. **95**, 1497 (2012)
19. D. Han, J. Zhang, P. Liu, G. Li, S. Wang, J. Eur. Ceram. Soc. **38**, 3261 (2018)
20. P.R. Bueno, R. Tararan, R. Parra, E. Joanni, M.A. Ramírez, W.C. Ribeiro, E. Longo, J.A. Varela, J. Phys. D-Appl. Phys. **42**, 55404 (2009)
21. J. Ghijsen, L.H. Tjeng, J.V. Elp, H. Eskes, J. Westerink, G.A. Sawatzky, M.T. Czyzyk, Phys. Rev. B **38**, 11322 (1988)
22. L. Ni, X.M. Chen, Appl. Phys. Lett. **91**, 122905 (2007)
23. A.N. Kamlo, J. Bernard, C. Lelievre, D. Houivet, J. Eur. Ceram. Soc. **31**, 1457 (2011)
24. J. Li, M.A. Subramanian, H.D. Rosenfeld, C.Y. Jones, B.H. Toby, A.W. Sleight, Chem Mater **16**, 5223 (2004)
25. F.D. Morrison, D.C. Sinclair, A.R. West, J. Am. Ceram. Soc. **84**, 474 (2001)
26. M.A. Ponce, M.A. Ramirez, F. Schipani, E. Joanni, J.P. Tomba, M.S. Castro, J. Eur. Ceram. Soc. **35**, 153 (2015)
27. M.H. Whangbo, M.A. Subramanian, Chem. Mater. **18**, 3257 (2006)
28. W.L. George, R.E. Grace, J. Phys. Chem. Solids **30**, 881 (1969)